Research Article

SURFACE and INTERFACE ANALYSIS

Received: 23 February 2010 Revised: 11 June 2010 Accepted: 12 June 2010 Published online in Wiley Interscience:

(www.interscience.wiley.com) DOI 10.1002/sia.3667

Micro/nanotribological behaviors of ionic liquid nanofilms with different functional cations

Wenjie Zhao,[a,b] Liping Wang,[a]* Mingwu Bai[c] and Qunji Xue[a]

Four kinds of molecularly thin films of room temperature ionic liquids (RTILs) with different functional cations were prepared on silicon substrates by dip-coating method. Thermal stability of the RTILs was evaluated using Mettler thermal gravity analysis (TGA) in a nitrogen atmosphere. Chemical compositions of the RTIL nanofilms were examined by means of multifunctional XPS. Nanoscaled adhesion and friction forces between the films and AFM tip were measured by FFM whereas the morphologies of the films were also investigated. Microscaled friction and wear behaviors between the films and Si_3N_4 ball were further measured by the microtribometer. The micro/nanotribological behaviors of different RTIL films were comparatively investigated and discussed in terms of functional cations of the RTILs molecules. Results in this paper revealed that the functional cations of the RTIL films significantly affected their tribological behaviors both in micro- and nanoscales. The corresponding micro/nanotribological mechanism of the tested ultrathin RTIL films under the test conditions was consequently proposed based on the experimental results.

Keywords: micro/nanofriction; ionic liquids; ultrathin films; functional cations; AFM

Introduction

Room-temperature ionic liquids (RTILs) are synthetic salts with a melting point at or below room temperature. They were initially developed by electrochemists for usage as electrolytes in batteries or for metal electrodeposition. It is possible to consider an artist's palette of anions and cations being used to create a vast range of ionic liquids, the anions being chosen to control the chemical properties,[1] and the cations being chosen to tailor the related physical properties.[2] As a nonconventional class of novel solvents, RTILs are becoming increasingly important and of particular interest in a wide range of research fields. They are a promising class of new materials with a bright technological future. These materials are now being used in applications that are enabled by their presence. Many of these applications involve electrochemistry, organic synthesis, catalysis chemistry, photochemistry and separation science for extraction of heavy metal ions, as green solvents for wide range of synthesis etc.[3–8] which make them particularly attractive. This is attributed to their interesting features such as no measurable vapor pressure, a broad liquid range, nonflammable and noncorrosive, tunable viscosity and electrochemical window, thermally and hydrolytically stable, excellent solvents for organic, inorganic and polymeric materials and electrical conductivity.

Recently, RTILs have aroused particular interest as potential lubricants, as their strong electrostatic bonding compared to covalently bonded fluids, leads to very desirable lubricating performance. So far, RTILs have been evaluated extensively, using conventional friction and wear tests. Previous researches have identified RTILs as great potential candidates for lubricants because RTILs exhibited excellent friction reduction, better antiwear resistance and high load-carrying capacity for a large amount of sliding pairs[9–13] such as steel/steel, steel/aluminum, steel/copper, steel/silica, etc. The tribological properties and thermal stability of RTILs are much more superior to that of conventional lubricants, such as PFPE and X-1P, etc.[9,12,14–16]

Micro/nanoelectromechanical systems (M/NEMS) devices are typically fabricated with silicon-based materials because mature lithographic fabrication techniques are available from the semiconductor industry. However, silicon and its native oxide exhibit high friction and poor antiwear performance in sliding contacts. Despite great progress in surface micromachining technology, as the size of mechanical systems shrinks from macro- to nanoscales, the surface-to-volume ratio increases, and consequently, surface phenomena such as adhesion, friction and wear remain key issues and big challenges for the realization and reliability of many M/NEMS devices.[17,18] To overcome these problems mentioned above, various nanofilms such as self-assembled monolayers (SAMs) are being developed and extensively studied, yet their reliability and feasibility remain in question.[17,19,20] Thin protective coatings are subject to wear during operation, limiting device lifetime.[21]

It is well known that nonvolatile lubricants with high thermal stability and a wide liquid range are required for advanced integrated circuit engines and M/NEMS. In order to improve tribological performance, RTILs are being considered for M/NEMS

* *Correspondence to: Liping Wang, State Key Laboratory of Solid Lubrication, Lanzhou Institute of Chemical Physics, Chinese Academy of Sciences, Lanzhou 730000, China. E-mail: lpwang@licp.cas.cn*

a *State Key Laboratory of Solid Lubrication, Lanzhou Institute of Chemical Physics, Chinese Academy of Sciences, Lanzhou 730000, China*

b *Graduate School of Chinese Academy of Sciences, Beijing 100039, China*

c *Department of Mechanical & Aerospace Engineering, George Washington University, Ashburn VA20147, USA*

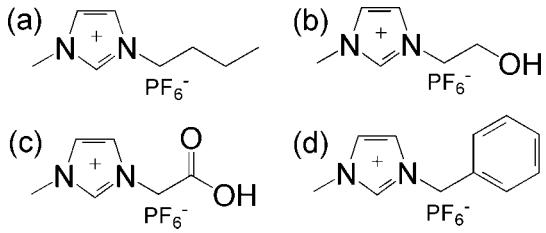

Figure 1. Chemical structures of the RTIL molecules.

applications because of their above mentioned unique characteristics and superior lubrication properties. Given the wide range of possible cation and anion combinations, the ionic components could be easily modified by specific functional groups to allow for a large variety of useful applications for related RTILs.

In the field of RTILs, our focus was placed on the fabrication of new functional cations-containing RTILs based on imidazolium cation, and subsequent investigation of their applications as novel lubricants. In previous work, we have investigated the effect of the anion and cation on the micro/nanotribological behaviors of several kinds of RTIL nanofilms.[22–26] However, the influence of terminal functional groups on micro/nanotribological behaviors of RTIL films has not been systemically examined yet. Because different cations can apparently affect micro/nanotribological performance of RTIL nanofilms,[27–30] in this work, we report the micro/nanotribological bahaviors of a series of RTILs with different functional cations when applied as ultrathin films, which allows an indepth understanding of the relationship between the cations and micro/nanotribological performance of RTIL nanofilms. Obtaining information on the molecular details of these new materials is of great importance for improving their properties and performances.[31–32] Four kinds of RTIL nanofilms were chosen due to their different functional cations: two with polar cations, such as –OH and –COOH, and the other two with apolar cations, such as $-CH_3$ and –Phenyl.

Experimental

Materials

Four kinds of RTILs (purchased from Chengjie Chemical Co. Ltd, Shanghai, purity ≥99%) including 1-butyl-3-methylimidazolium hexafluorophosphate, 1-ethanol-3-methylimidazolium hexafluorophosphate, 1-acetic acid-3-methylimidazolium hexafluorophosphate and 1-phenyl-3-methyl-imidazolium hexafluorophosphate abbreviated as [BMIM]PF6, [EtOHMIM]PF6, [MCOOHMIM]PF6 and [PhMIM]PF6, respectively. The chemical structures of the RTILs used in this study were schematically shown in Fig. 1. P-doped single-side polished single-crystal silicon (100) wafers (obtained from GRINM Semiconductor Materials Co. Ltd., Beijing) with a surface roughness of about 0.2 nm, and a thickness of 0.5 mm were used as the substrate. All the other reagents of analytical grade were used as received.

Pretreatment of silicon wafers

All glass vials used were cleaned by thoroughly rinsing with deionized (DI) water and acetone and then dried at 100 °C in an oven. Cleaned silicon wafers were ultrasonicated in acetone followed by ethanol for 10 min each, and then immersed in a freshly prepared piranha solution (volume ratio of 7 : 3 mixture of 98% H_2SO_4 and 30% H_2O_2) at 90 °C for 40 min to produce hydroxyl groups on the surfaces. Then the substrates were rinsed with DI water and blown dry with nitrogen flow.

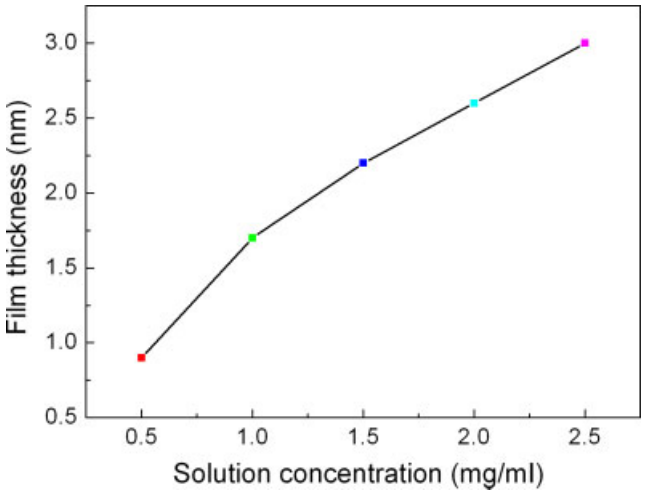

Figure 2. Relationship between the concentration of [BMIM]PF6 and the thickness of its film on silicon surface.

Film preparation

Solutions of RTILs were prepared in acetone at different concentrations. The silicon wafer was slowly dipped into a tank containing the solution and then withdrawn from it with a velocity of 60 μm/s after being immersed in the solution for 120 sec. Si wafer was allowed to dry in air in a clean room prior to the following measurements. As shown in Fig. 2, the thickness of the films is in proportion to the concentration of the solution. According to this relationship, it is easy to prepare RTIL nanofilms with a certain thickness. In order to compare the micro/nanotribological properties of RTIL nanofilms with different molecular structures, the thickness of all the RTIL films prepared in this study is kept at approximately 3 nm.

RTILs and films characterization

The thermal stability of RTILs and Zdol-3800 were examined by thermogravimetric analysis (TGA) between 20 and 800 °C, a constant heating rate of 10 °C/min and high-purity argon purge were used for all the measurements.

The film thickness was determined using an ellipsometer (L116-E, Gaertner, USA) equipped with a He-Ne laser ($\lambda = 632.8$ nm) at a fixed incidence angle of 50°. The thickness was recorded from 10 locations on each sample.

XPS is a highly diagnostic tool for the assessment of the chemical state of elements. In this paper, a PHI-5702 mutifunctional XPS was applied for the determination of the chemical compositions and structures of the silicon surfaces coated with RTIL nanofilms. As parameters, a pass energy of 29.35 eV, Mg–Kα ($h\nu = 1253.6$ eV) radiation for excitation and a take-off angle of 36° were used. Chamber pressure was about 3×10^{-8} Torr. Electron binding energies were calibrated using the contaminated carbon (C1s: 285.0 eV)

Nanotribological characteristics measurements

AFM/FFM is widely used in nanotribology and nanomechanics studies.[27,33,34] In this paper, nanotribological behaviors of RTIL

SURFACE and INTERFACE ANALYSIS

nanofilms were characterized with an AFM/FFM controlled by CSPM4000 electronics, using the contact mode. Commercially available rectangle silicon cantilevers with a nominal spring constant, 40 N/m, a curvature radius of about 30 nm, and rear side coated with aluminum (Budgetsensors Instrument Inc.) was employed.

To study the frictional properties of the surfaces, a variation of torsion deflections were detected according to the well established protocol.[35,36] To obtain friction data, the tip was scanned back and forth in the x direction in contact with the sample, while the lateral deflection of the lever was measured. The differences in the lateral deflection or friction signal between back and forth motions is proportional to the friction force. Friction forces were continuously measured with various external loads. The load was increased linearly in each successive scan line. Scanning for the friction force measurement was performed at the rate of 1 Hz along the scan axis and a scan size of 1 μm × 1 μm. The sets of data were displayed graphically in a friction image.

Adhesion forces were measured between the AFM tip and RTIL nanofilms by recording the cantilever deflection in the force-displacement (attraction/retraction) curves. The adhesive force (F) which is also called pull-off force was calculated by

$$F = KcZp$$

Where Kc is the force constant of cantilever and Zp is the vertical displacement of the piezotube.[37,38]

To minimize the variability of the tip shape, the same tip was used throughout the investigation. Reliable pull-off force measurements were obtained by averaging 10 data points per sample by recording the force-displacement curves at different locations on the surface. All the experiments were performed at a relative humidity level of 30–40% at room temperature.

Microtribological characteristics measurements

The microfriction and wear properties of all these RTIL nanofilms were evaluated using a UMT-2MT microtribometer operating in the reciprocating mode. Si_3N_4 ball of 3.18 mm in diameter was selected as the counterpart. Figure 3 shows the surface morphology of the Si_3N_4 ball used in this study. The root mean square (RMS) roughness of the ball was estimated to be about 28.6 nm. The Si_3N_4 ball was fixed in a stationary holder sustained by a beam, and the samples were then mounted on a reciprocating table. The ball moved horizontally with respect to the sample surface with a sliding frequency between 1 and 4 Hz and a traveling distance of 5 mm. Applied normal loads used were between 60 and 400 mN and the change in the friction coefficient was monitored vs sliding time or cycles. The initiation of wear on the sample surface leads to an increase in the friction coefficient, and a sharp increase was interpreted to indicate film failure. The friction coefficient and sliding time were recorded automatically by a computer, and at least three repeated measurements were performed. All the tests were conducted at room temperature and at a relative humidity of 30–40%.

Results and Discussion

Thermal behavior RTILs

TGA curves of Zdol and RTILs are shown in Fig. 4. It is observed that all RTILs show little weight loss below 300 °C, which corresponds

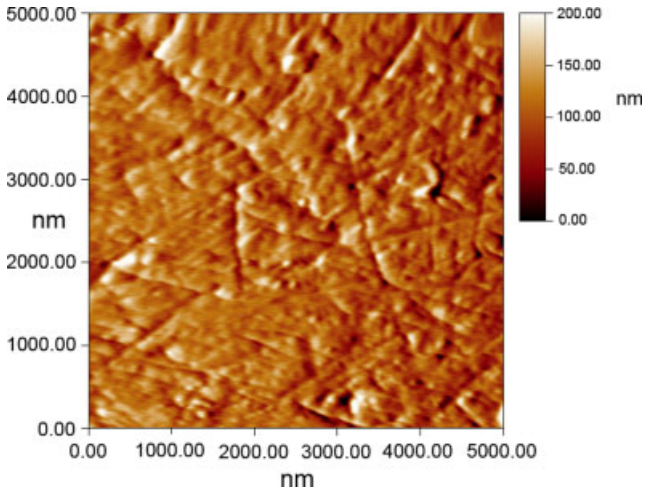

Figure 3. AFM morphology of the Si_3N_4 ball surface.

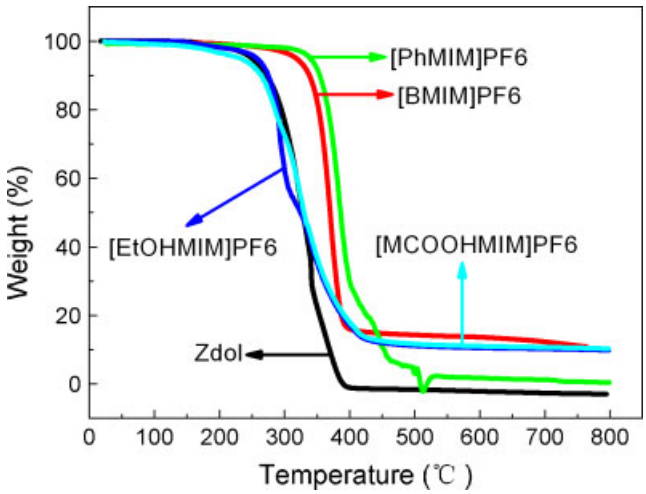

Figure 4. TGA curves of Zdol and RTILs.

to the extremely low vapor pressures of RTILs and, hence, meets the demands of a high-performance lubricant. Compared to Zdol-3800, RTILs show relatively better performance in terms of thermal stability. Further, it is observed that thermal degradation of [PhMIM]PF6 starts at 350 °C and then completes at 500 °C. [PhMIM]PF6 exhibited the best performance in terms of thermal stability among all the lubricants. Compared to –Phenyl cation, the thermal stability of other functional cations such as –OH, –COOH, $-CH_3$ significantly decreased. It is assumed that functional cations demonstrated great effect on the thermal stability of RTILs.

Composition and morphology

XPS analysis was used to further clarify the chemical states of several typical elements of boundary film formed on the silicon surfaces lubricated with RTILs with different functional cations. The changes in elemental composition could clearly prove whether the reagents were deposited on the silicon wafer surfaces or not. Figure 5 showed the XPS scan survey spectra of RTIL nanofilms. Each scan survey spectra demonstrated the characteristic elements, for example: F_{1s} at 685.1 eV, N_{1s} at 400.2 eV and P_{2p} at 133.3 eV were observed clearly, which indicates that all RTIL nanofilms were coated successfully on the silicon surface.

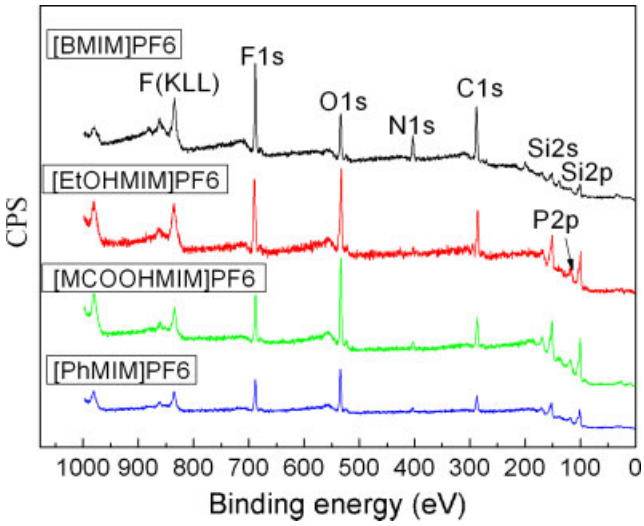

Figure 5. XPS spectra of RTIL nanofilms.

Figure 6(a–d) shows 2D and 3D AFM images for a bare Si wafer before and after treatment by piranha solution. It can be clearly observed that the bare Si wafer is smooth and uniform with a RMS roughness of 0.18 and 0.14 nm before and after treatment by piranha solution, respectively. AFM morphological images of [BMIM]PF6, [EtOHMIM]PF6, [MCOOHMIM]PF6 and [PhMIM]PF6 nanofilms are presented in Fig. 7(a–h). As seen from Fig. 7(a–h), the [BMIM]PF6, [EtOHMIM]PF6 and [MCOOHMIM]PF6 nanofilms prepared on the silicon surface at room temperature are quite uniform and continuous. But the [PhMIM]PF6 film is not quite uniform and continuous, there are some microaggregates formed on the silicon surface. However, from a macropoint, both RTIL nanofilms are homogenously distributed on the silicon surface. The RMS roughness of [BMIM]PF6, [EtOHMIM]PF6, [MCOOHMIM]PF6 and [PhMIM]PF6 films is about 0.13, 0.13, 0.1 and 0.17 nm, respectively.

Adhesive force measurements under ambient conditions

The adhesive forces measured on the RTIL nanofilms with different functional cations are summarized in Fig. 8, Si (100) data were also provided for a comparison. As depicted in Fig. 8, [PhMIM]PF6 exhibited the lowest adhesive force, whereas, Si–OH showed the largest adhesive force. The adhesive force decreased in the sequence of Si–OH, [EtOHMIM]PF6, [MCOOHMIM]PF6, and [BMIM]PF6, to [PhMIM]PF6. In other words, altering the cations, for instance, from apolar ones (–CH3 and –phenyl) to polar ones (–COOH, –OH), results in an increase of the adhesion force. The reason for the difference in adhesion force is that RTILs with more polarized groups generally possess higher surface energy and, consequently, exhibited hydrophilic properties.

It is well known that, hydrophilic lubricant films easily formed a meniscus by themselves or by the adsorbed water molecules, which results in a higher adhesive force due to the capillary effect. In turn, hydrophobic lubricant films show low adhesion.[39,40] [EtOHMIM]PF6 and [MCOOHMIM]PF6 contain polar cations which are hydrophilic, so they demonstrated relatively higher adhesive force. On the contrary, [BMIM]PF6 and [PhMIM]PF6 containing apolar cations are hydrophobic, so they exhibit lower adhesive force.

Nanotribological properties

To study the nanofriction properties of RTIL nanofilms with different functional cations, the friction force vs normal load with different tip sliding velocity curves were measured by AFM/FFM

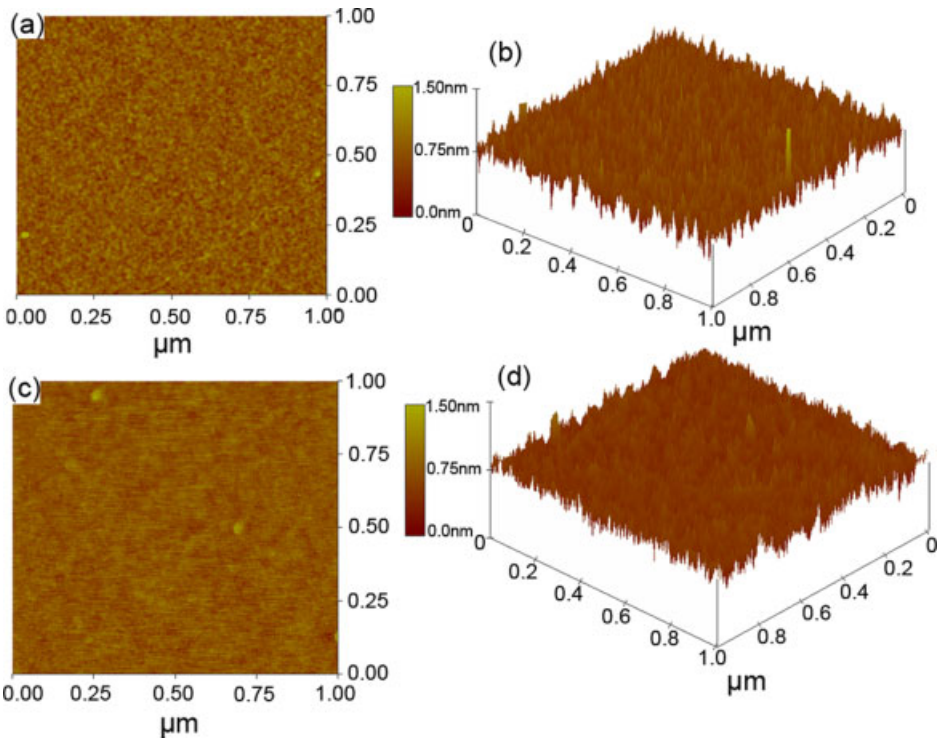

Figure 6. 2D and 3D AFM images of (a) and (b) bare Si before treatment by piranha solution; and (c) and (d) bare Si after treatment by piranha solution.

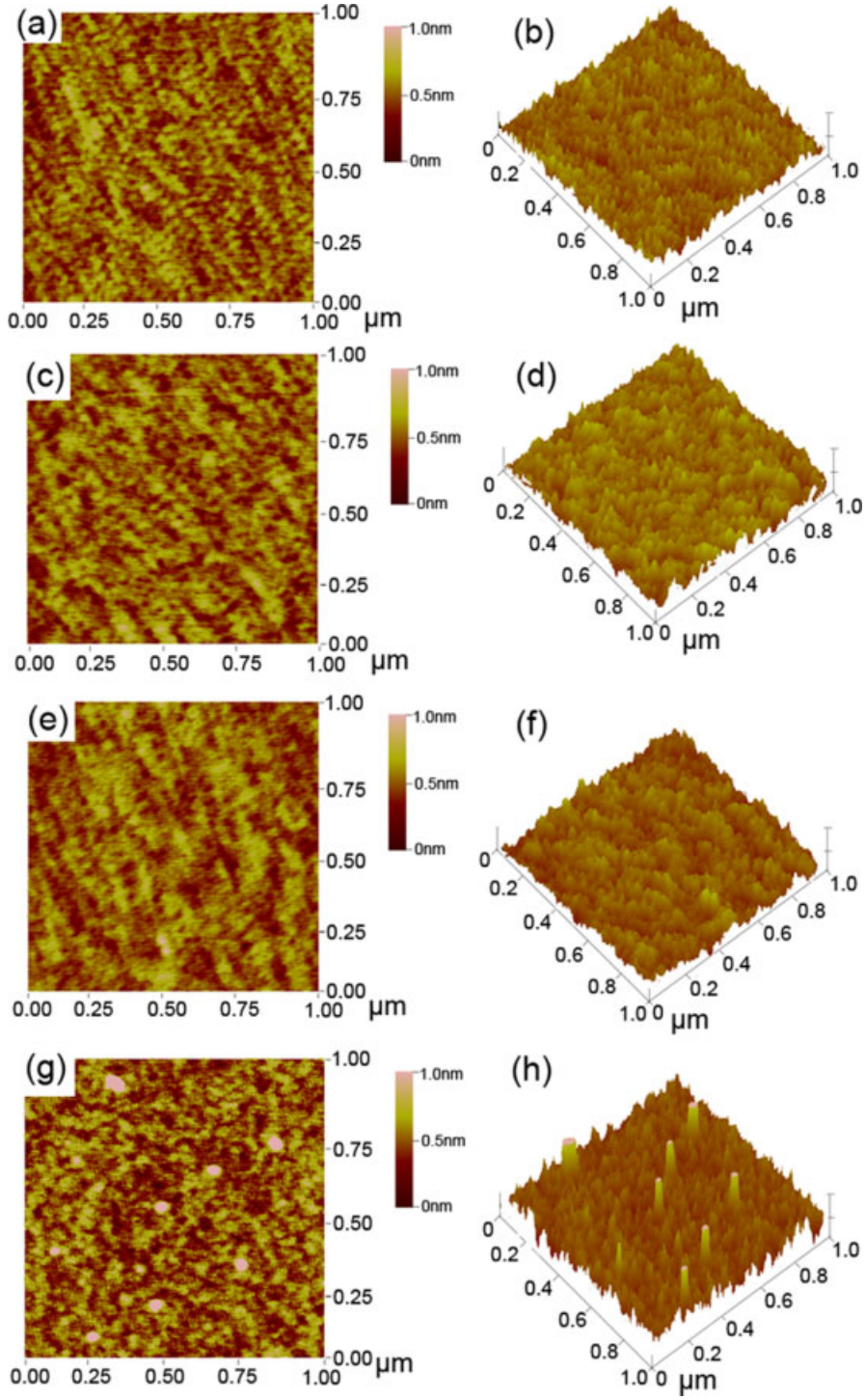

Figure 7. 2D and 3D AFM images of nano-films of (a) and (b) [BMIM]PF6; (c) and (d) [EtOHMIM]PF6; (e) and (f) [MCOOHMIM]PF6; and (g) and (h) [PhMIM]PF6.

under increased normal loads. The influence of sliding velocity and functional cation on the nanofriction force was investigated as shown in Fig. 9. The friction force of [EtOHMIM]PF6 nanofilm was larger than the other three kinds of RTIL nanofilms, and [BMIM]PF6 film showed the lowest friction force. Furthermore, the friction forces of RTIL films were found to change with the increasing of tip sliding velocity.

Hydrophilic lubricant films, such as [EtOHMIM]PF6 and [MCOOHMIM]PF6 are easily formed a meniscus by themselves or the adsorbed water molecules. This provides greater resistance for tip sliding and leads to the higher friction force due to the capillary force. On the contrary, hydrophobic lubricant films such as [BMIM]PF6 and [PhMIM]PF6 show relatively lower friction force.[39,40] As for the comparison between [BMIM]PF6 and [PhMIM]PF6, the higher stiffness of the ring backbone, as compared to the compliant chain backbone, is believed to result in the higher friction for [PhMIM]PF6 than that for [BMIM]PF6 under the same load and sliding velocity.[41,42] For the special ring backbone, it is

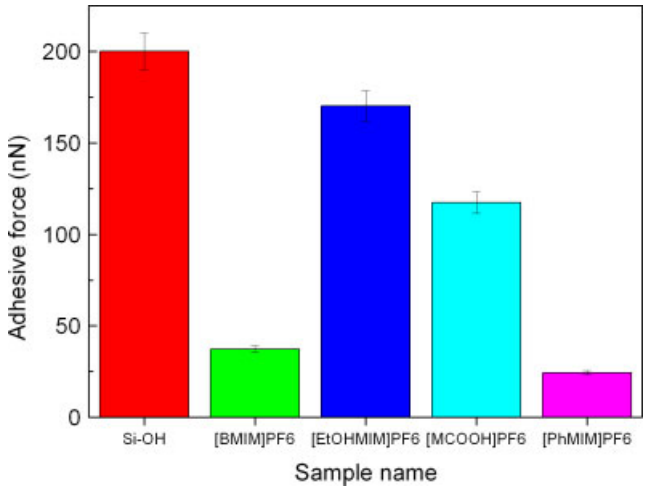

Figure 8. Adhesive force between AFM tip and different RTIL nanofilms.

harder to rotate due to the stiffness of the ring structure. On the other hand, the compliant chain can rotate more freely. So the RTILs molecules with higher spring constant or stiffer backbone structure may need more energy to be elastically deformed during sliding. Therefore, friction force is higher for these kinds of RTIL nanofilms. As the tip proceeds along the scan direction at low scanning velocity, RTILs molecules are 'relieved' from the tip load and reorient to their initial position. But as velocity increased, fewer molecules had sufficient time to reorient, and these molecules are now opposed to the tip motion.[43,44] Thus, at higher velocities, the friction force of RTIL film was higher when the tip was returning.

Microfriction and antiwear properties

The antiwear ability of RTIL nanofilm is very important for their potential use as a lubricant layer. Figure 10(a–d) shows the plot of friction coefficients with sliding time of RTIL nanofilms with different functional cations.

For [BMIM]PF6 film, as shown in Fig. 10(a), the average friction coefficient was approximately 0.11 at the normal load of 60 mN. When the normal load was increased to 80 mN, the average friction coefficient decreased to about 0.08 and remained stable even after sliding for 3500 s. With the increase of normal load, durability of the [BMIM]PF6 film decreased dramatically, and it failed instantly at a load of 100 mN only sliding for 175 s. The above results indicated that [BMIM]PF6 nanofilm exhibited poor antiwear performance at high loads.

As shown in Fig. 10(b), [EtOHMIM]PF6 film was recorded at a friction coefficient of 0.08, which was kept almost constant at a load of 100 mN. When the normal load increased to 200 mN, the friction coefficient slightly decreased to 0.03, which was still almost stable under all sliding cycles. Even at a sliding load of 400 mN, the friction coefficient still kept stable at 0.05 during the whole sliding time.

In Fig. 10(c), an average friction coefficient of about 0.2 was observed for [MCOOHMIM]PF6 film at a low load of 100 mN. When the normal load was increased to 200 mN, the friction coefficient slightly decreased to 0.17, which was still almost stable under all sliding cycles. But the friction coefficient abruptly increased at a sliding load of 400 mN after only sliding for 250 s, indicating that severe wear loss of the [MCOOHMIM]PF6 film occurred and resulted in the subsequent failure of the nanofilm.

Figure 10(d) shows the variation of friction coefficients and durability of [PhMIM]PF6 film on Si substrates against Si_3N_4 ball

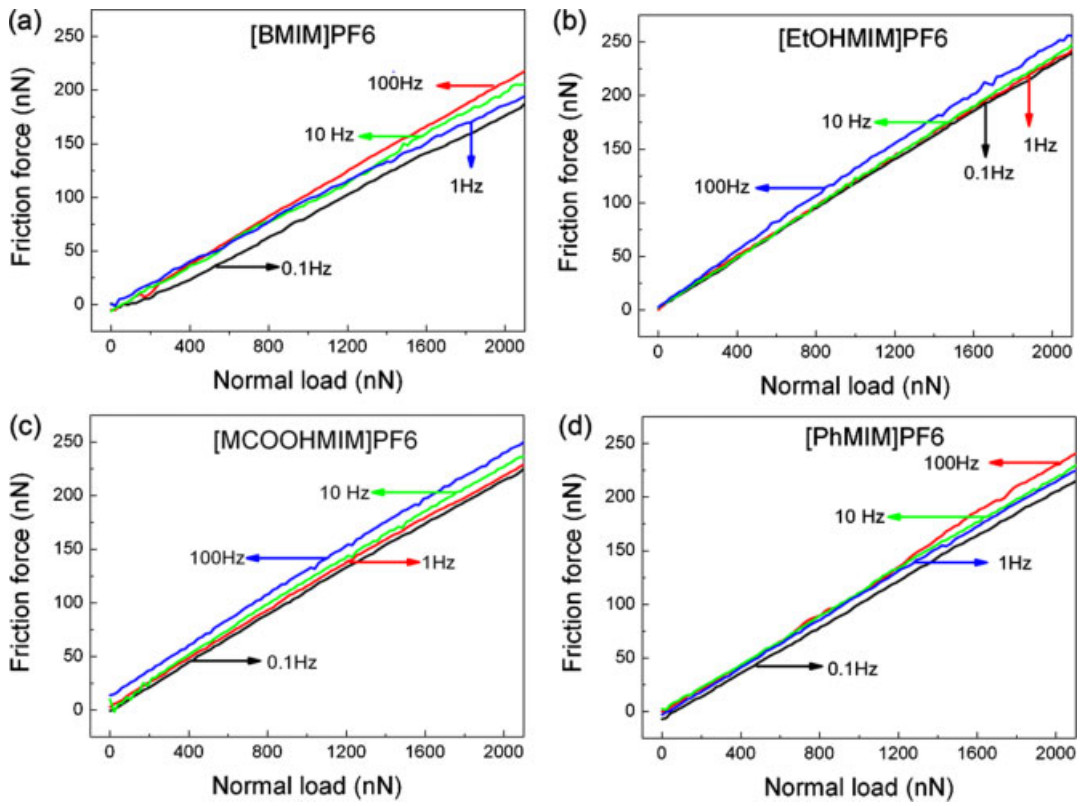

Figure 9. Plots of nanofriction force vs applied loads for (a) [BMIM]PF6; (b) [EtOHMIM]PF6; (c) [MCOOHMIM]PF6; and (d) [PhMIM]PF6 nanofilms.

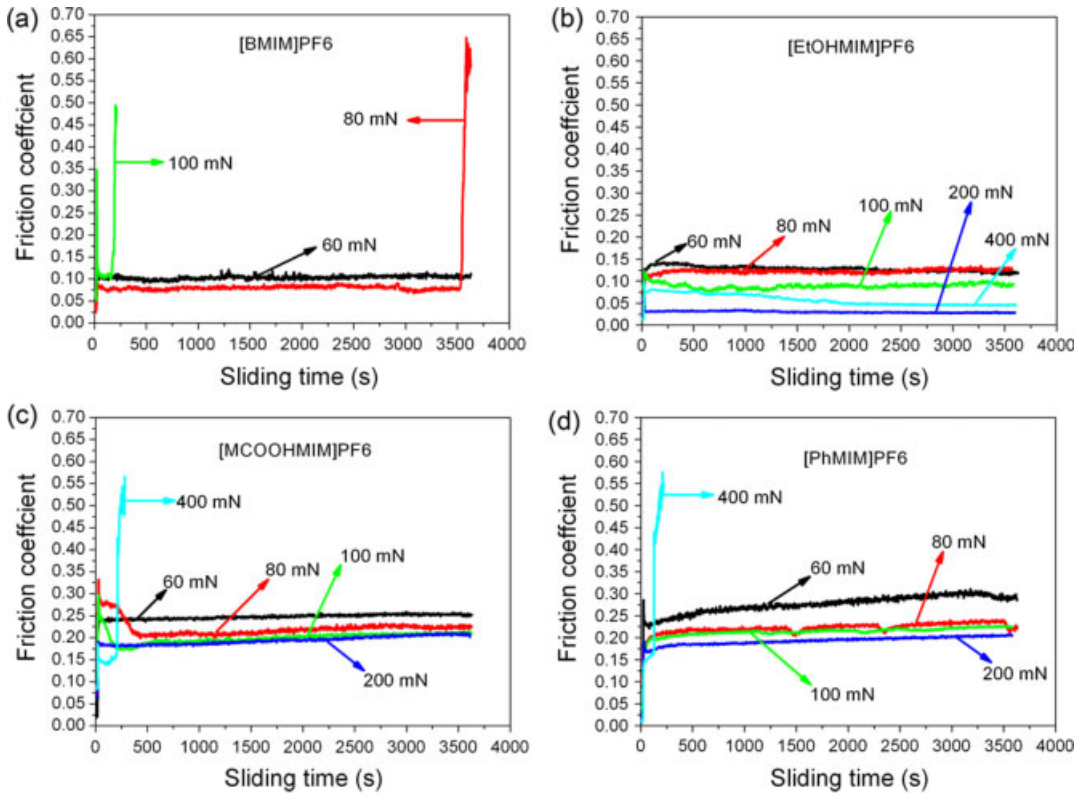

Figure 10. Variation in friction coefficient with sliding time for RTIL nanofilms at different applied loads (a) [BMIM]PF6; (b) [EtOHMIM]PF6; (c) [MCOOHMIM]PF6; and (d) [PhMIM]PF6.

with sliding time. It can be seen that [PhMIM]PF6 film was recorded at an average friction coefficient about 0.24 under a load of 60 mN. When the normal load was increased to 80 or 100 mN, the average friction coefficient decreased to about 0.2 and remained stable even after sliding for 3600 s. An average friction coefficient of about 0.17 was observed for [PhMIM]PF6 film at a low load of 200 mN, and remained stable even after sliding for 3600 s. When the normal load was increased to 400 mN, the average friction coefficient increased sharply to 0.6 just after sliding for 110 s, which indicated that the friction reduction effect by [PhMIM]PF6 nanofilm diminished under the test condition.

From the above results, it can be concluded that the functional cations of RTILs strongly affected their microfriction properties. RTIL films with functional cations, such as [EtOHMIM]PF6, [MCOOHMIM]PF6 and [PhMIM]PF6 nanofilms exhibited longer durability and higher load bearing capacity than that for [BMIM]PF6 film in the load range. But [BMIM]PF6 film exhibited lower friction coefficient than other three kinds of RTIL films. Between RTIL films with carboxylic acid and phenyl-terminated spacer chains or alkyl chains structure, the higher stiffness of the carboxylic acid and phenyl spacer chains as compared to the compliant alkyl chains was believed to result in the higher friction coefficient for [MCOOHMIM]PF6 and [PhMIM]PF6 films than [BMIM]PF6 film under the same load and sliding velocity.[41,42,45] For the carboxylic acid and phenyl spacer chains, it required a larger external force to allow orientation due to the stiffness of structure. On the other hand, compliant alkyl chains rotated more freely. So, the RTILs molecules with higher spring constant or stiffer backbone structure may need more energy to be elastically deformed during sliding. The enhanced antiwear and load carrying ability of [EtOHMIM]PF6, [MCOOHMIM]PF6 and [PhMIM]PF6 films should rely on their functional cations. It can be concluded that the optimum choice of the functional cations can greatly improve their microtribological properties.

For micro/nanofilms, the frictional coefficient during friction process normally could be affected by the sliding velocity. The average coefficients for the [BMIM]PF6, [EtOHMIM]PF6, [MCOOHMIM]PF6 and [PhMIM]PF6 nanofilms during the initial 20 min for each sliding frequency were collected. As shown in Fig. 11, the friction coefficients of all the RTIL nanofilms varied with the increase of sliding frequency, but not a monotonous increase or decrease. It has contributed to the higher degree of oscillation and distortion of the molecules at higher shear velocity, which accelerates the dissipation of the accumulated energy and is a complicated process.[46]

Conclusions

Four kinds of RTIL films with different functional cations were successfully prepared, and then their composition and microstructure were characterized. The micro/nanotribological behaviors of these RTIL nanofilms were systematically investigated. On the basis of the experimental results, it is observed that RTIL nanofilms with polar or stiff phenyl cations exhibited relatively higher friction force and better antiwear performance than the ones with apolar alkyl chain structure at micro/nanoscale. The different micro/nanofriction performances of the RTIL nanofilms were mainly dependent on their different cations which mainly influence their hydrophobic/hydrophilic properties. Adhesive force was also determined by the hydrophobic/hydrophilic properties of RTILs' functional cations. Since RTIL nanofilms with more polarized groups

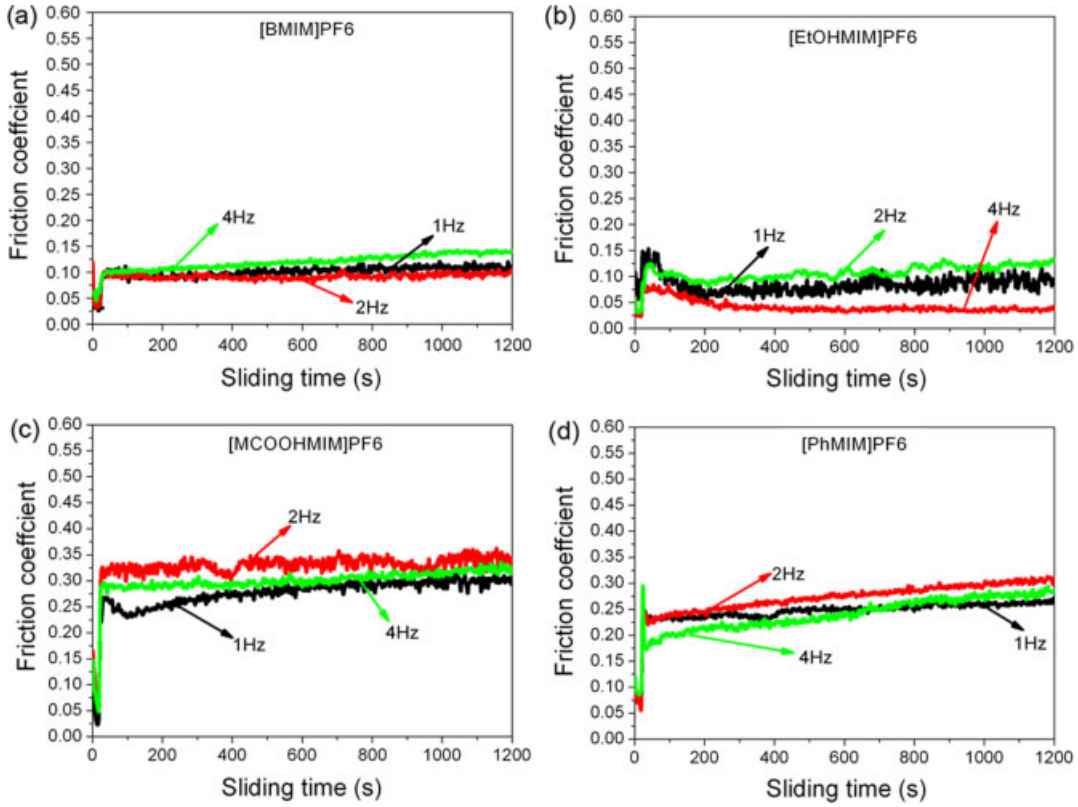

Figure 11. Variation in friction coefficient with sliding velocity for (a) [BMIM]PF6; (b) [EtOHMIM]PF6; (c) [MCOOHMIM]PF6; and (d) [PhMIM]PF6 nanofilms at a normal load of 60 mN.

generally possessed higher surface energy and a relatively strong interaction during the sliding, and therefore, higher adhesion and more energy loss are expected, which lead to a higher friction force. The friction force was also found to vary with the increase of tip sliding velocity. The results in this paper indicated that RTIL nanofilms demonstrated strong potential as lubricant for M/NEMS because they have better thermal stability than traditional PFPE lubricants and desirable tribological properties both under micro- and nanoscaled friction regime.

Acknowledgements

The authors thank the National Natural Science Foundation of China (Grant Nos 20773148 & 50905178), and the 863 Program of Chinese Ministry of Science and Technology (No. 2009AA03Z105).

References

[1] M. J. Earle, S. P. Katdare, K. R. Seddon, *Org. Lett.* **2004**, *6*, 707.
[2] K. R. Seddon, A. Stark, M. J. Torres, *ACS Symp. Ser.* **2002**, *819*, 34.
[3] M. Mominullslam, T. Ohsaka, *J. Electroanal. Chem.* **2008**, *623*, 147.
[4] W. Thomas, *Chem. Rev.* **1999**, *99*, 2071.
[5] M. J. Earle, P. B. McCormac, K. R. Seddon, *Chem. Commun.* **1998**, *20*, 2245.
[6] D. Haristoy, D. Tsiourvas, *Chem. Mater.* **2003**, *15*, 2079.
[7] A. E. Visser, R. P. Swatloski, W. M. Reichert, R. Mayton, S. Sheff, J. H. Davis, R. D. Rogers. Jr, *Chem. Commun.* **2001**, *1*, 135.
[8] G. Q. Yu, F. Zhou, W. M. Liu, Y. M. Liang, S. Q. Yan, *Wear* **2006**, *260*, 1076.
[9] C. F. Ye, W. M. Liu, Y. X. Chen, L. G. Yu, *Chem. Commun.* **2001**, *1*, 2244.
[10] M. H. Yao, Y. M. Liang, Y. Q. Xia, F. Zhou, *ACS Appl. Mater. Interfaces.* **2009**, *1*, 467.
[11] X. Q. Liu, F. Zhou, Y. M. Liang, W. M. Liu, *Wear* **2006**, *261*, 1174.
[12] F. Zhou, Y. M. Liang, W. M. Liang, *Chem. Soc. Rev.* **2009**, *38*, 2590.
[13] W. J. Zhao, L. P. Wang, M. W. Bai, Q. J. Xue, *Colloids Surf. A* **2010**, *361*, 118.
[14] M. Zhu, Y. F. Mo, W. J. Zhao, M. W. Bai, *Surf. InterfaceAnal.* **2009**, *41*, 205.
[15] Y. Q. Xia, S. J. Wang, F. Zhou, H. Z. Wang, Y. M. Lin, T. Xu, *Tribol. Int.* **2006**, *39*, 635.
[16] G. X. Xie, Q. Wang, L. N. Si, S. H. Liu, G. Li, *Tribol. Lett.* **2009**, *36*, 247.
[17] B. Bhushan, T. Kasai, G. Kulik, L. Barbieri, P. Hoffmann, *Ultramicroscopy* **2005**, *105*, 176.
[18] V. V. Tsukruk, *Adv. Mater.* **2001**, *13*, 95.
[19] H. S. Ahn, P. D. Cuong, S. K. Park, Y. W. Kim, J. C. Lim, *Wear* **2003**, *255*, 819.
[20] M. Masuko, H. Miyamoto, A. Suzuki, *Tribol. Int.* **2007**, *40*, 1587.
[21] D. B. Asay, M. T. Dugger, J. A. Ohlhausen, S. H. Kim, *Langmuir* **2008**, *24*, 155.
[22] W. J. Zhao, M. Zhu, Y. F. Mo, M. W. Bai, *Colloids Surf. A* **2009**, *332*, 78.
[23] W. J. Zhao, Y. F. Mo, J. B. Pu, M. W. Bai, *Tribol. Int.* **2009**, *42*, 828.
[24] M. Zhu, J. Yan, Y. F. Mo, M.W. Bai, *Tribol. Lett.* **2008**, *29*, 177.
[25] Y. F. Mo, B. Yu, W. J. Zhao, M. W. Bai, *Appl. Surf. Sci.* **2008**, *255*, 2276.
[26] Y. F. Mo, W. J. Zhao, M. Zhu, M. W. Bai, *Tribol. Lett.* **2008**, *32*, 143.
[27] N. J. Brewer, B. D. Beake, G. J. Leggett, *langmuir* **2001**, *17*, 1970.
[28] H. I. Kim, M. Graupe, O. Oloba, T. Koini, S. Imaduddin, T. R. Lee, S. S. Perry, *Langmuir* **1999**, *15*, 3179.
[29] H. I. Kim, T. Koini, T. R. Lee, S. S. Perry, *Langmuir* **1997**, *13*, 7192.
[30] J. E. Houston, C. M. Doelling, T. K. Vanderlick, Y. Hu, G. Scoles, I. Wenzl, T. R. Lee, *Langmuir* **2005**, *21*, 3926.
[31] M. Palacio, B. Bhushan. *Adv. Mater.* **2008**, *20*, 1194.
[32] H. S. Ahn, P. D. Cuong, S. K. Park, Y. W. Kim, J. C. Lim, *Wear* **2003**, *255*, 819.
[33] B. Bhushan, A. V. Kulkarni, V. N. Koinkar, M. Boehm, L. Odoni, C. Martelet, M. Belin, *Langmuir* **1995**, *11*, 3189.
[34] N. J. Brewer, G. J. Leggett, *Langmuir* **2004**, *20*, 4109.
[35] Y. S. Shon, S. Lee, R. C. Jr, S. S. Perry, T. R. Lee, *J. Am. Chem. Soc.* **2000**, *122*, 7556.
[36] S. Lee, Y. S. Shon, R. C. Jr, R. L. Guenard, T.R. Lee, S. S. Perry, *Langmuir* **2000**, *16*, 2220.

[37] S. Yang, H. Zhang, S. M. Hsu, *Langmuir* **2007**, *23*, 1195.
[38] S. K. Sinha, M. Kawaguchi, T. Kato, F. E. Kennedy, *Tribol. Int.* **2003**, *36*, 217.
[39] S. H. Kim, D. B. Asay, M. T. Dugger, *Nanotoday* **2007**, *2*, 22.
[40] B. Bhushan, *Handbook of Micro/Nano tribology* (2nd edn), CRC Press, Boca Raton, FL, **1999**.
[41] N. S. Tambe, B. Bhushan, *Nanotechnology* **2004**, *15*, 1561.
[42] N. S. Tambe, B. Bhushan, *Nanotechnology* **2005**, *16*, 1549.
[43] J. I. Siepmann, I. R. McDonald, *Phys. Rev. Lett.* **1993**, *70*, 453.
[44] M. Garcia-Parajo, C. Longo, J. Servat, P. Gorostiza, F. Sanz, *Langmuir* **1997**, *13*, 2333.
[45] H. W. Liu, B. Bhushan, *Ultramicroscopy* **2002**, *91*, 185.
[46] S. L. Ren, S. R. Yang, J. Q. Wang, W. M. Liu, Y. P. Zhao, *Chem. Mater.* **2004**, *16*, 428.

